Available online at www.sciencedirect.com

ScienceDirect

Advances in Climate Change Research xxx (xxxx) xxx

www.keaipublishing.com/en/journals/accr/

Understanding the physical processes in the evolution of a cold air outbreak over China in late November 2022 from a Lagrangian perspective

Jin-Ning CHE[a], Bo LIU[a,b,c,*], Shang-Feng LI[d,**], Cheng YOU[e], Kara HARTIG[f], Lei CHEN[a,c]

[a] *Department of Atmospheric Science, School of Environmental Studies, China University of Geosciences, Wuhan 430074, China*
[b] *State Key Laboratory of Severe Weather, Chinese Academy of Meteorological Sciences, Beijing 100081, China*
[c] *Centre for Severe Weather and Climate and Hydro-Geological Hazards, Wuhan 430074, China*
[d] *Jilin Provincial Key Laboratory of Changbai Mountain Meteorology and Climate Change, Laboratory of Research for Middle–High Latitude Circulation Systems and East Asian Monsoon, Institute of Meteorological Sciences of Jilin Province, Changchun 130062, China*
[e] *Alfred Wegener Institute, Helmholtz Centre for Polar and Marine Research, Potsdam 14473, Germany*
[f] *Department of Physics, Harvard University, Cambridge 02138, USA*

Received 31 March 2023; revised 19 June 2023; accepted 28 August 2023

Abstract

From 26 November to 1 December 2022, intense cold air masses swept across China from northwest to south, resulting in a nationwide cold air outbreak (CAO) case characterised by drastic and sudden temperature drops with rain, snow and strong winds. The physical processes that dominate the intensification of the cold air masses during this CAO event remain unclear. In this study, the evolution of the CAO case, which is indicated by the dry static energy (DSE), is investigated using a novel approach in the framework of Lagrangian backtracking. The dominant processes can be identified by decomposing the DSE change into four diabatic heating terms due to shortwave radiation, longwave radiation, latent heat and turbulent processes. Overall, in this case, most of the cold air parcels originated from the east of Novaya Zemlya and crossed Central Siberia before reaching China. Thus, these air parcels mainly manifested on the northwest–southeast path. The duration of the cold air intensification differed between subregions. The cold air parcels experienced long cooling periods (approximately 9 d) before reaching northern China (i.e. Northwest, North and Northeast China), whilst the southern parts (i.e. Central, East and South China) underwent relatively short cooling periods (6–8 d). Accordingly, the cold air affecting northern China is more intense than that affecting the southern parts, especially for East and South China. For all six subregions, longwave radiative cooling is identified as the dominant contributor to the cold air intensification, and the latent heat processes as the secondary contributor. The weakening of cold air parcels as they approach and pass over these regions is driven by turbulent processes and shortwave heating. Central Siberia and Lake Baikal are identified as key areas for the intensification of cold air passing over both regions. In addition, air parcels affecting Northwest China are intensely cooled as they pass over the Junggar Basin, while the North China Plain is a key area for cooling air parcels reaching Central, East and South China. From a Lagrangian perspective, these findings provide insights into the physical processes driving the behaviour of cold air parcels, which would help understand the mechanisms involved in the past changes and future projections in CAOs.

Keywords: Cold air outbreak; HYSPLIT; Dry static energy; Temperature tendency; Diabatic heating

1. Introduction

Cold air outbreaks (CAOs) are high-impact weather and climate events that have destructive impacts on transport, agriculture, energy infrastructure and human health (Cohen et al., 2014; Ding et al., 2020; Li et al., 2022; Zhang et al.,

* Corresponding author. Department of Atmospheric Science, School of Environmental Studies, China University of Geosciences, Wuhan 430074, China.
** Corresponding author.
E-mail addresses: boliu@cug.edu.cn (LIU B.), ice-lsf@163.com (LI S.-F.).
Peer review under responsibility of National Climate Center (China Meteorological Administration).

https://doi.org/10.1016/j.accre.2023.08.009
1674-9278/© 2023 The Authors. Publishing services by Elsevier B.V. on behalf of KeAi Communications Co. Ltd. This is an open access article under the CC BY-NC-ND license (http://creativecommons.org/licenses/by-nc-nd/4.0/).

Please cite this article as: CHE, J.-N et al., Understanding the physical processes in the evolution of a cold air outbreak over China in late November 2022 from a Lagrangian perspective, Advances in Climate Change Research, https://doi.org/10.1016/j.accre.2023.08.009

2022). The northern midlatitude continents, such as North America (Screen and Simmonds, 2014; Wallace et al., 2014) and East Asia (Liu et al., 2012; Gong et al., 2014; Luo et al., 2020), have experienced increasingly serious and frequent, even record-breaking CAOs. These abrupt CAOs frequently lead to super-low temperatures, snow freezing disasters (Ding et al., 2008), high economic losses (Sun et al., 2018; Ma and Zhu, 2019; Dai and Mu, 2020) and abnormal stress on the energy supply and power system (Li et al., 2022; Liu et al., 2022). In particular, the increasingly serious consequences of CAOs are widespread and severe in populous regions such as China due to the high exposure of personnel and infrastructure (Huang et al., 2021; X. Li et al., 2022). Therefore, focusing on the evolutionary mechanisms of these high-impact CAOs is important for disaster prevention and mitigation.

Isentropic potential vorticity analysis (Hoskins et al., 1985; Iwasaki et al., 2014) is currently applied to identify the accumulation and movement of cold air masses and describe their outbursts (Ding and Ma, 2007; Huang et al., 2020; Liu et al., 2020; Tao and Zheng, 2012; Yamaguchi et al., 2019). For example, Shoji et al. (2014) investigated the temporal evolution of CAOs in the East Asian winter monsoon, defined by the equatorward flux of cold air masses below a potential temperature of 280 K across the 45°N range from 90°E to 180°, covering 30 winters from 1980 to 2009.3D trajectory methods (Walsh et al., 2001; Sun et al., 2017; Wang et al., 2017), such as the FLEXible PARTicle dispersion model and the Hybrid Single-Particle Lagrangian Integrated Trajectory (HYSPLIT) model, are another approach that can be used to track the movement and temperature changes for individual air parcels. Cai et al. (2019) tracked the trajectories of 46 cold wave events affecting North China from 1961 to 2014 and clustered them into three types matching different atmospheric circulation characteristics. Several studies have focused on the temperature evolution altered by various adiabatic and diabatic processes as cold air parcels travel. The changes in potential temperature along the trajectories from the outputs of the Lagrangian model only help infer the total diabatic heating due to the difficulty in identifying specific diabatic mechanisms (Papritz et al., 2015; Papritz and Spengler, 2017; Hermann et al., 2020). These previous studies recognising the formation and physical evolution of CAOs consolidate the foundation for subsequent further investigations.

Lagrangian backward trajectories and decomposition for the diabatic heating term are jointly used to further identify specific diabatic heating mechanisms responsible for the temperature changes of cold air parcels in detail (You et al., 2020, 2021, 2022; Hartig et al., 2023). Examining the details of specific diabatic heating mechanisms using this method helps improve the understanding and forecasting of the CAOs. Using the output from a climate model, CESM1.2 (CAM5), to drive the HYSPLIT model, Hartig et al. (2023) selected the vertical mixing term, which dominates the diabatic cooling of the air parcels and contributes to the North American cold events. However, observational (reanalysis) datasets have not been used within this framework to investigate the specific physical processes related to the observed CAO cases.

From 26 November to 1 December 2022, China was recently hit by a serious nationwide CAO, which has been chosen as one of the Top 10 Weather and Climate Events in China in 2022 due to its remarkable impact characterised by drastic and sudden temperature drops with rain, snow and strong winds (CMA, 2023). Yao et al. (2023) demonstrated that this extreme CAO and several other ones during November−December 2022 were closely related to the formation of blocking circulations and the phase transition of the North Atlantic Oscillation. Observational (reanalysis) datasets were combined with the decomposition for the diabatic heating term to analyse the specific physical processes related to this CAO case. Several issues in this extreme CAO remain to be addressed: 1) What were the dominant pathways of the cold air parcels that hit China during this CAO case? 2) Which diabatic processes dominated the strengthening of cold air parcels? 3) When and where did the cold air accumulate and intensify?

This study aims to gain a comprehensive understanding of the evolution of cold air parcels, using this case as an example, within the Lagrangian framework, with an emphasis on revealing the dominant processes that result in the strengthening of cold air parcels. Identifying the key physical processes and areas of cold air intensification is important for the prediction of CAO, as well as disaster prevention and mitigation.

2. Data and methodology

2.1. Observed and reanalysis datasets

The daily minimum temperature at 2414 meteorological stations in China, obtained from the CMA, was used to detect the CAO. The input data for the HYSPLIT model were from the latest ECMWF reanalysis dataset (ERA5; Hersbach et al., 2020). The variables used have a time resolution of 1 h and a horizontal resolution of 0.75°, including three-dimensional variables (such as geopotential height, zonal and meridional wind, specific humidity and vertical pressure velocity) and two-dimensional fields (such as terrestrial height and 10-m zonal and meridional wind). The total temperature tendency, that is, the temperature tendency term due to all parametrisations, two other temperature tendency terms due to shortwave and longwave radiation and the specific humidity tendency due to parametrisations at 1 h interval (https://confluence.ecmwf.int/display/CKB/ERA5%3A+data+documentation) were also utilised to investigate the detailed processes involved in the CAO.

2.2. Identification of cold air outbreak (CAO)

The adapted Chinese national standard on the grade of cold waves (GB/T 21987-2008; CMA, 2017) is used to identify CAO events. The first criterion is the single station CAO, i.e. a daily minimum temperature drop $\geq$8 °C, $\geq$10 °C or $\geq$12 °C in 24, 48 and 72 h, respectively. The 24 h (48 or 72 h) temperature drop was defined by subtracting the minimum

Please cite this article as: CHE, J.-N et al., Understanding the physical processes in the evolution of a cold air outbreak over China in late November 2022 from a Lagrangian perspective, Advances in Climate Change Research, https://doi.org/10.1016/j.accre.2023.08.009

temperature of the previous day (two or three days before) from the current day. Regional CAO criterion is that more than 40% of the total meteorological stations in the target region fall within the standard of the single station CAO criterion.

2.3. Trajectory simulations of cold air parcels with HYSPLIT

The HYSPLIT model, which was developed by the National Oceanic and Atmospheric Administration (NOAA) Air Resources Laboratory (ARL; Draxler and Hess, 1997, 1998; Stein et al., 2015), was used to calculate the backward trajectories for the cold air parcels. The movement of an air parcel is the integration of its position vector through space and time in the model. The HYSPLIT was utilised to facilitate the backward tracking of air parcels in the target regions (i.e. the six subregions in Fig. 1) when the regional CAO criterion is satisfied. The backward simulation was initiated four times with a 6 h interval at 0000, 0600, 1200 and 1800 Beijing Local Time to minimise the overlap in these trajectories for each subregion for every CAO day. The model then integrated a 10-d backward trajectory starting at 100 m above ground level (AGL) for each target grid at each initial moment. The output of the HYSPLIT model is recorded at 1 h interval and includes the three-dimensional position (i.e. latitude, longitude and AGL), terrain height and ambient and potential temperatures of the air parcels.

2.4. Decomposition of temperature tendency in the Lagrangian framework

Similar to that in Hartig et al. (2023), the concept of dry static energy (DSE) was used to determine the dominant diabatic processes in the development of cold air parcels in this case.

$$DSE = c_p T + gz, \tag{1}$$

where T is the air temperature, g is the gravitational acceleration, c_p is the specific heat of the air, and z is the geopotential height. The DSE is conserved during adiabatic expansion or compression; therefore, the evolution of the DSE is all attributed to diabatic processes. Furthermore, in the Lagrangian framework, following an air parcel, the contribution of dynamical processes from the advection effect to the DSE tendency can be safely eliminated. Therefore, the evolution of the DSE is nearly due to physical processes. In the following, the DSE is given the unit of temperature by dividing c_p to conveniently demonstrate the contribution of diabatic processes. As described by You et al. (2021), the rate of temperature change ($\dot{T}_{\mathrm{Physics}}$; i.e. the hourly-mean temperature tendency in this study) can be decomposed into four components due to different physical processes, as shown below.

$$\dot{T}_{\mathrm{Physics}} = \dot{T}_{\mathrm{SW}} + \dot{T}_{\mathrm{LW}} + \dot{T}_{\mathrm{LH}} + \dot{T}_{\mathrm{Turbulent}}, \tag{2}$$

where $\dot{T}_{\mathrm{SW}}$ and $\dot{T}_{\mathrm{LW}}$ are the temperature tendencies due to the local heating/cooling by shortwave and longwave radiation, respectively. $\dot{T}_{\mathrm{LH}}$ denotes the temperature tendency due to the latent heat release, which is calculated from the tendency of specific humidity due to parameterised processes ($\dot{q}$) as,

$$\dot{T}_{\mathrm{LH}} = -L_v \dot{q}, \tag{3}$$

where L_v is the latent heat of vaporisation. The $\dot{T}_{\mathrm{Turbulent}}$ is then calculated as the residual term, i.e. the subtraction of the three

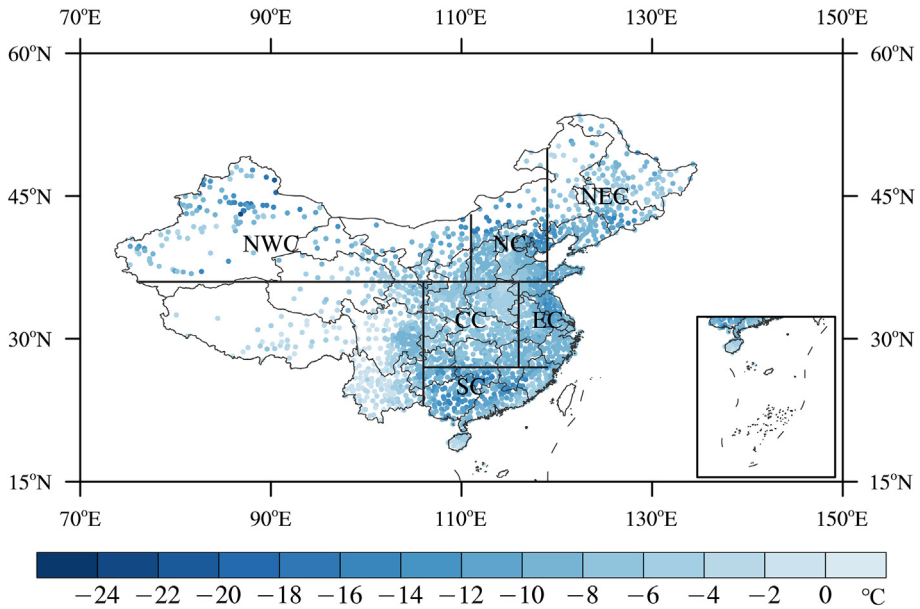

Fig. 1. Spatial distribution of maximum 24 h drop in daily minimum temperature at 2414 stations across China and the following six subregions (Northwest China (36°−46°N, 75°−111°E), North China (36°−46°N, 111°−119°E), Northeast China (39°−54°N, 119°−134°E), Central China (27°−36°N, 106°−116°E), East China (27°−36°N, 116°−122°E) and South China (20°−27°N, 106°−120°E)).

Please cite this article as: CHE, J.-N et al., Understanding the physical processes in the evolution of a cold air outbreak over China in late November 2022 from a Lagrangian perspective, Advances in Climate Change Research, https://doi.org/10.1016/j.accre.2023.08.009

other components ($\dot{T}_{SW}$, $\dot{T}_{LW}$ and $\dot{T}_{LH}$) from the total temperature tendency ($\dot{T}_{Physics}$), encompassing the effect of vertical turbulent heat transport and the latent heat release due to turbulent process-induced specific humidity tendency. Therefore, in the Lagrangian framework, i.e. along the trajectory of air parcels,

$$\Delta DSE \approx \int \dot{T}_{Physics} dt = \int \dot{T}_{SW} + \dot{T}_{LW} + \dot{T}_{LH} + \dot{T}_{Turbulent} dt. \quad (4)$$

2.5. Interpolation of temperature tendencies

To quantify contributions of individual processes in Eq. (4) to the change in DSE along the trajectory, the temperature tendency terms were interpolated to the trajectory positions simulated by the HYSPLIT using the procedure from the official website.[1] The details are as follows. Firstly, each tendency term at all 137 model levels from the ERA5 dataset is interpolated to 136 pressure levels, from 220 to 1050 hPa (1050 to 1026 hPa at 1 hPa intervals, 1025 to 1000 hPa at 2.5 hPa intervals, 995 to 500 hPa at 5 hPa intervals and 490 to 220 hPa at 10 hPa intervals). The temperature tendencies at the pressure levels were then interpolated, position by position, to the trajectory according to their four-dimensional coordinates (i.e. time, pressure, latitude and longitude). Therefore, the dominant processes and the key areas favouring the intensification/weakening of the air parcels were identified.

3. Results

3.1. Overview of the cold air outbreak case and the synoptic situation

The extreme CAO, driven by upstream Eurasian blocking, swept across continental China from 26 November to early December. As the blockage intensified and transformed into a Ural blocking, the edge of the low-pressure trough reached northern Xinjiang (Yao et al., 2023), and the associated cold air inflow initially caused a sharp temperature reduction of around 8−20 °C in this region on 26 November (Fig. 2a). Consistent with the gradual shift of the east−west low-pressure trough to the north−south, the cold air masses behind the trough spread rapidly southward and eastward to cover most of the country, including Inner Mongolia and northern, northeastern, Central and southern China, from 27 to 30 November 2022 (Fig. 2b−e). As the trough moved further east, the CAO ended on 1 December (Fig. 2f). Approximately 50% of the stations had a maximum 24 h temperature drop of 8 °C during this CAO case, with 472 (accounting for 19.85% of the total) stations witnessing a drop of 10 °C. The largest 24 h temperature drop of 20.2 °C was recorded at the Qinghe station in Xinjiang.

The vast areas affected by this CAO case were divided into six subregions for a comprehensive investigation, as shown in Fig. 1 (NRC, 2007). The dates of the identified regional CAOs are as follows: 27−29 November 2022 for Northwest China; 28−30 November 2022 for North China and East China; 29 November 2022 for Northeast China; 29−30 November 2022 for Central China; and 29 November to 1 December 2022 for South China. As mentioned above, the 10-d backward simulation with the HYSPLIT is initiated four times at their CAO days for each region. Overall, 6828, 1800, 1240, 1352, 1212 and 1812 trajectories were obtained for Northwest, North, Northeast, Central, East and South China, respectively. Only some tracked air parcels led to CAOs. Therefore, 'effective trajectory' is defined as a detection criterion in which the last DSE is larger than any of the DSE at the final 24, 48 or 72 h along the trajectory. Based on the concept of 'effective trajectory', 2419, 811, 404, 674, 946 and 1164 trajectories were finally selected for Northwest, North, Northeast, Central, East and South China, respectively.

3.2. Pathways of cold air parcels and the associated temperature evolution

Tracing the origins and pathways of cold air parcels helps understand their evolution. As indicated by the distribution of trajectory frequencies in Fig. 3, cold air parcels during this case originated mainly from the east of Novaya Zemlya, and most trajectories passed through the 'key area for cold air outbreak' (KA hereafter), i.e. Central Siberia (43°−65°N, 70°−90°E) before their final arrival in six target regions. Therefore, these air parcels manifested on the northwest-to-southeast path, with the exception of Northwest China, which is roughly a north-to-south path.

For the North China, two main pathways for cold air parcels from the KA are found. The dominant one in the north, termed the 'KA-Baikal route', moved east across Lake Baikal and then turned south to North China via the Mongolian Plateau (Fig. 3b). Meanwhile, a small group of trajectories along Xinjiang and Inner Mongolia to North China was termed the 'KA-Xinjiang−Inner Mongolia route'. The spatial pattern of trajectory frequencies for Central and South China resembled that for North China. However, the 'KA-Xinjiang−Inner Mongolia route' dominates for Central China, while both routes are almost equally important for South China (Fig. 3d and f, respectively). By contrast, the trajectories reaching Northeast and East China had only one main pathway that moved from the KA to Lake Baikal and then south to their destination regions (Fig. 3c and e, respectively).

As mentioned in Section 2, the increase/decrease in DSE can be used as an indicator of diabatic heating/cooling, respectively, for air parcels. As indicated in Eq. (1), the DSE along the trajectory is calculated using air temperature and geopotential height (terrain geopotential height plus AGL). The highly similar evolution, with correlation coefficients greater than 0.98 for six subregions, between potential temperature, output directly from the HYSPLIT, and DSE, proves the validity of using DSE to study the diabatic processes. As

[1] https://confluence.ecmwf.int/display/CKB/ERA5%3A+compute+pressure+and+geopotential+on+model+levels%2C+geopotential+height+and+geometric+height.

Please cite this article as: CHE, J.-N et al., Understanding the physical processes in the evolution of a cold air outbreak over China in late November 2022 from a Lagrangian perspective, Advances in Climate Change Research, https://doi.org/10.1016/j.accre.2023.08.009

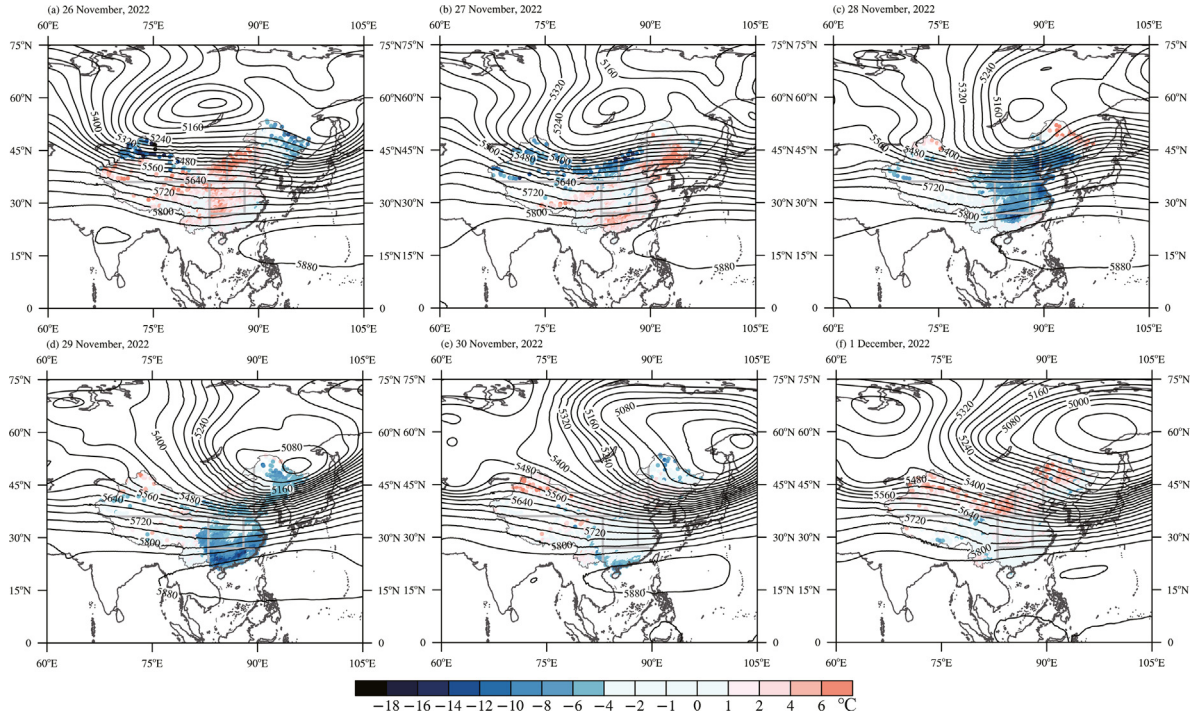

Fig. 2. Spatial distribution of 24 h temperature change of 2414 stations across China (shading) and 500 hPa geopotential height (contours, unit: gpm) from 26 November to 1 December 2022.

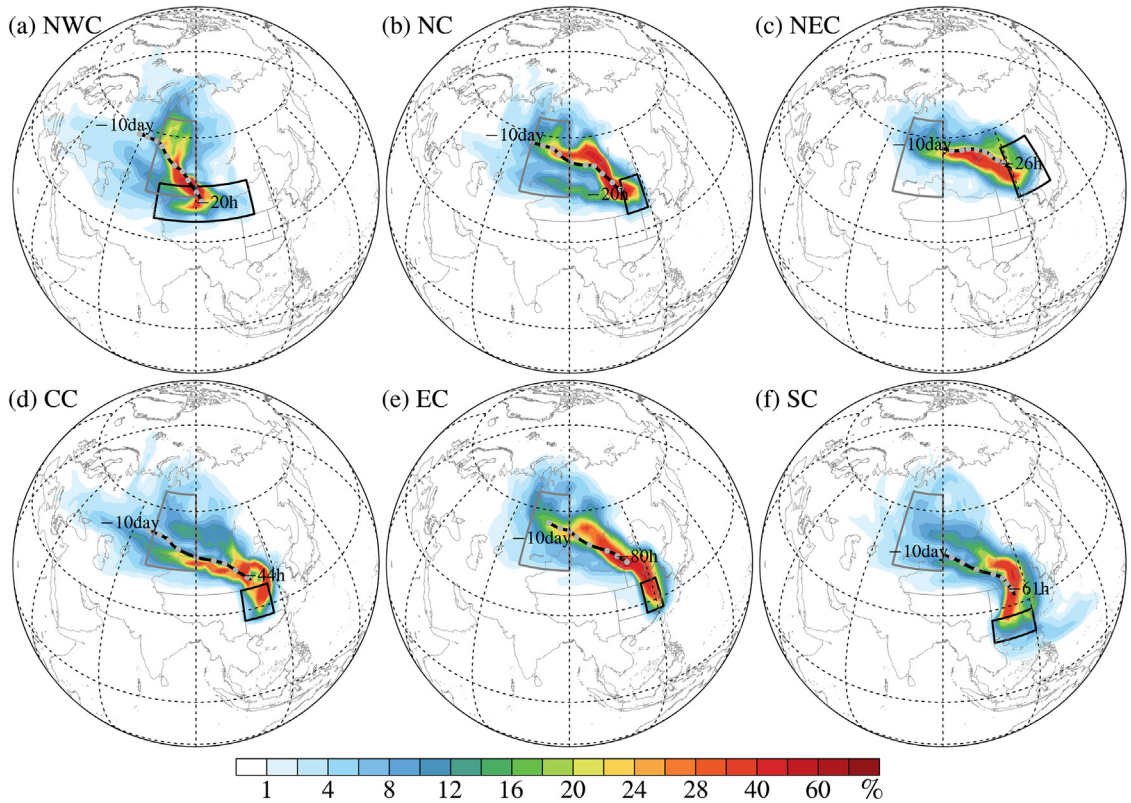

Fig. 3. Spatial distribution of the trajectory frequencies (shading) for all effective trajectories to (a) Northwest China, (b) North China, (c) Northeast China, (d) Central China, (e) East China and (f) South China (The black box indicates the six subregions. The grey box indicates Central Siberia. The black curve represents the averaged 10-d backward trajectory for all air parcels, and the grey dots denote the locations of air parcels from −10 d to the strongest cold air accumulation, with a time resolution of 1 d).

Please cite this article as: CHE, J.-N et al., Understanding the physical processes in the evolution of a cold air outbreak over China in late November 2022 from a Lagrangian perspective, Advances in Climate Change Research, https://doi.org/10.1016/j.accre.2023.08.009

shown in the evolution of DSE (Fig. 4a), air parcels were generally cooled for the first 7 d and then heated slightly over the final 3 d. The cooled periods correspond to the intensification of cold air parcels, whilst the heated periods indicate the outburst of cold air, that is, the heat exchange between cold air masses and the warm ground.

Therefore, the minimum DSE was used to indicate the cold peak of the cold air parcel before reaching the target region, and the intensification stage of cold air was defined as the period from −10 d to the moment with the minimum DSE. Notably, the minimum DSE refers to the minimum value of the DSE along the averaged backward trajectories for each subregion. The specific moments for the six subregions are −20 h (Northwest and North China), −26 h (Northeast China), −44 h (Central China), −80 h (East China) and −61 h (South China). The minus sign indicates the time before reaching the target region. The cold air parcels that attacked northern China

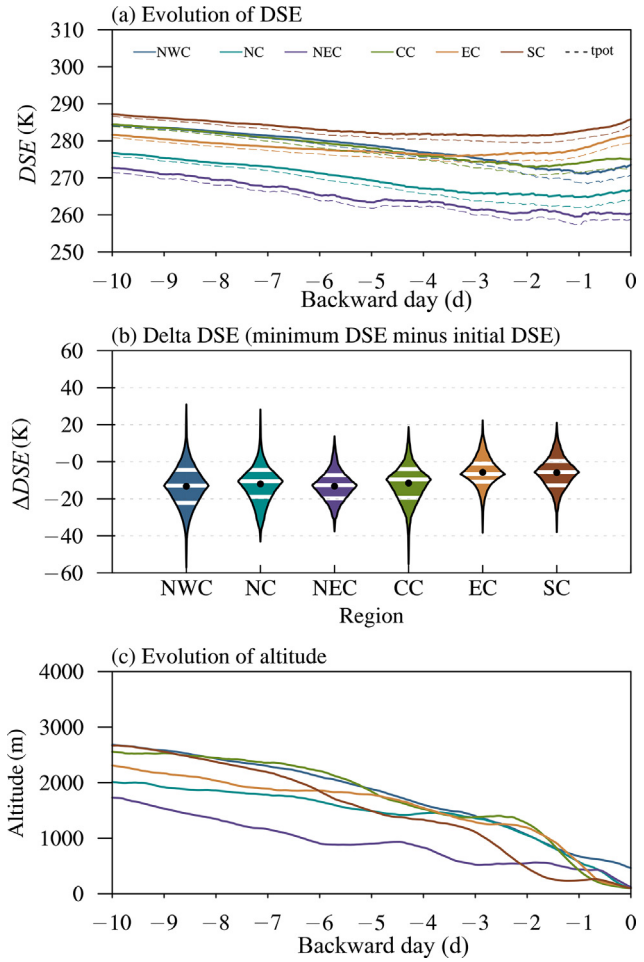

Fig. 4. (a) Evolution of dry static energy (DSE) (solid line) and potential temperature (dotted line) from 10-d prior (−10 d) to the moment that the air parcel reached the target grid (0 d) represented by the ensemble average for all effective trajectories in each region, (b) statistical characteristics of the average changes between the minimum and initial distribution of DSE in all air parcels from six subregions. (The box-percentile plot extends from the minimum to the maximum of the data, and the white marks represent the 25th, 50th and 75th percentile), and (c) averaged altitude for ensemble air parcels from each target region along the 10-d backward trajectories.

(i.e. Northwest, North and Northeast China) experienced long cooling periods of almost 9 d due to the short distance with polar regions. For the three other subregions in southern China, the cooling periods are 6−8 d, which is mainly due to the fact that these trajectories are the continue of those attacked the northern parts (Fig. 3). The relatively long periods for the cold air parcel to accumulate and intensify in this case are reported to be partly associated with the maintenance of Ural blocking, which is suggested to be associated with the significant negative anomalies in the meridional potential vorticity gradient over mid-high latitudes from North America to Eurasia (Luo et al., 2019; Yao et al., 2022, 2023). Corresponding to the long cooling periods, the intensification of cold air, indicated by the difference between the minimum DSE and the DSE at −10 d, is also strong for Northwest China (−13.3 K), North China (−12.0 K), Northeast China (−13.3 K) and Central China (−11.5 K). Conversely, the DSE of air parcels in South and East China only obtained reductions of 5.8 K and 5.9 K, respectively, after the slight and short accumulation of cooling processes (Fig. 4b).

The altitudes (geopotential height) of the backward trajectories for these regions have similar evolution characteristics over time, with an almost continuous descent from the polar to the target regions. The origin height (−10 d) of the cold air, in this case, is approximately 1800−2800 m, which is significantly higher than the initial height (100 m AGL) at the target region due to the complicated topography along the route (Fig. 4c).

3.3. Diabatic processes contributing to the development of cold air parcels

The evolution of DSE over 10 d before reaching the target regions is decomposed into four terms on the right-hand side in Eq. (4) and a residual term. The cumulative contribution of the distinct diabatic processes expressed by these terms is calculated along 10-d average backward trajectories. As illustrated in Fig. 5, the time-integrated contribution from the local cooling by longwave radiation dominates the decrease in DSE for all six subregions. On average, cold air parcels arriving at three northern subregions experienced a similar sustained magnitude of longwave radiation cooling at the arrival of the maximum change in cumulative DSE, roughly 20 K cooler, with a maximum cooling amplitude of 22 K in Northwest China (Fig. 5g). The negative contribution of shortwave radiation and the turbulent term to cold air parcels was smaller than the cooling effect of longwave radiation and latent heat release. These conditions drove the rapid accumulation of cold air in the Northwest, North and Northeast China during the previous 9 d along the trajectory.

Confirming the statement in Fig. 4b above, the DSE of air parcels moving towards East and South China accumulated more weakly than other subregions. They underwent gentle cooling by longwave radiation, only half as much as those in three northern regions at −11.8 K and −12.8 K. The contributions of latent heat release were −3.5 K over the trajectory reached in Northwest China and less than −2.0 K in five other

Please cite this article as: CHE, J.-N et al., Understanding the physical processes in the evolution of a cold air outbreak over China in late November 2022 from a Lagrangian perspective, Advances in Climate Change Research, https://doi.org/10.1016/j.accre.2023.08.009

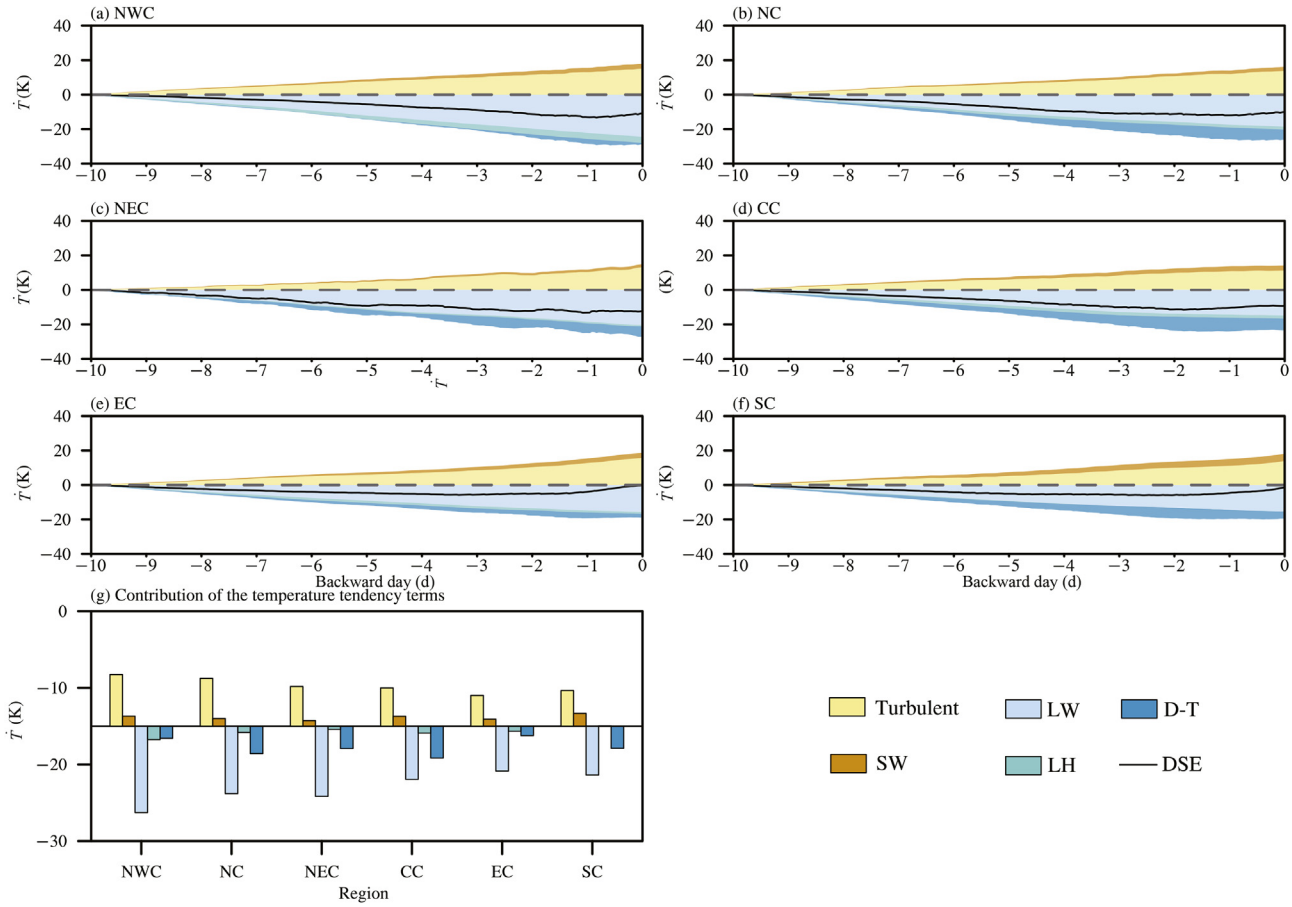

Fig. 5. (a–f) Evolution of the cumulative contributions from distinct diabatic processes ($\int \dot{T}_{\mathrm{LW}}\mathrm{d}t$; $\int \dot{T}_{\mathrm{Turbulrnt}}\mathrm{d}t$; $\int \dot{T}_{\mathrm{SW}}\mathrm{d}t$; $\int \dot{T}_{\mathrm{LH}}\mathrm{d}t$; $DSE - \int \dot{T}_{\mathrm{Physics}}\mathrm{d}t$) to DSE changes of air parcels in time, from 10 d prior to its arrival at the six target regions (At each time moment, the values of temperature tendency items are stacked one on top of the other, with the first data item added from the zero line. The contributions to air parcels cooling are coloured blue, while the others are coloured yellow), and (g) the cumulative contributions of distinct diabatic processes during the intensification stage, i.e. from −10 d to the moment with the maximum decrease in DSE, for each region.

subregions, which were almost negligible. The additional cooling was attributed to the residual term ranging from 2.5 K to 8.4 K. The turbulent term and shortwave heating were negative contributors to the evolution of the CAOs, which had the warming effect integrated over the first 180 h of trajectory to South China, offsetting 68.2% (+12.6 K versus −18.5 K) of the cooling. Furthermore, Table 1 shows that the standard deviation of the turbulent term along trajectories is of the order of 0.5 K h^{-1}, while the temperature tendency term of longwave radiation is around 0.2 K h^{-1}. The turbulent process may be an important factor in determining the variability of cold air parcels based on the similar standard deviations of the turbulent term and the DSE change.

Table 1
Average standard deviations of each temperature tendency term along the 10-d backward trajectories from six regions (unit: K h^{-1}).

Region	DSE change	LW	Turbulent	SW	LH
Northwest China	±0.58	±0.32	±0.56	±0.04	±0.11
North China	±0.49	±0.19	±0.45	±0.02	±0.07
Northeast China	±0.56	±0.18	±0.52	±0.01	±0.05
Central China	±0.42	±0.18	±0.39	±0.03	±0.11
East China	±0.38	±0.14	±0.36	±0.03	±0.12
South China	±0.42	±0.16	±0.40	±0.03	±0.18

3.4. Identification of key areas for cold air intensification

To identify the location where the cold air parcel was significantly cooled during the intensification stages, we defined the contribution fraction (CF) of each grid (i) to the total DSE decrease during the intensification as,

$$CF(i) = \frac{\sum_{i}(\Delta DSE)}{\sum_{1}^{n}\left(DSE_{\min} - DSE_{-10\mathrm{day}}\right)} \tag{5}$$

where $\sum_{i}(\Delta DSE)$ is the accumulated DSE changes for all air trajectories passing through grid i, with a resolution of 2.5°, and $\sum_{1}^{n}\left(DSE_{\min} - DSE_{-10\mathrm{day}}\right)$ is the total DSE reduction during the intensification stages for all effective trajectories (n). Therefore, the key areas could be identified as those with significantly large contribution fractions.

The spatial distribution of contribution fractions is shown in Fig. 6. Note that for better focus, only the grids with high

Please cite this article as: CHE, J.-N et al., Understanding the physical processes in the evolution of a cold air outbreak over China in late November 2022 from a Lagrangian perspective, Advances in Climate Change Research, https://doi.org/10.1016/j.accre.2023.08.009

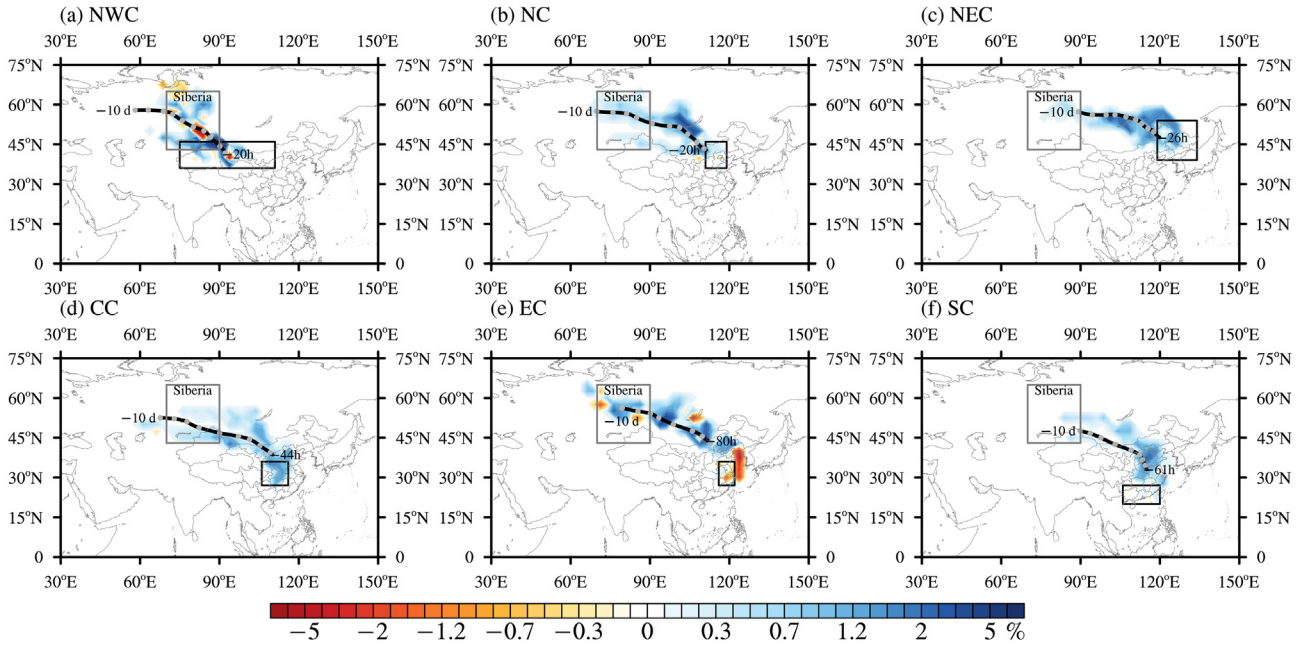

Fig. 6. Spatial distribution of regional contribution to the changes of DSE along each trajectory reaching the six subregions (The black box indicates the subregion. The grey box indicates Central Siberia. The black curve represents the average backward trajectory of all air parcels, and the grey dots denote the locations of the air parcels from −10 d to the cold air accumulated to its strongest, with a time resolution of 1 d).

trajectory frequencies of more than 10% are considered. Corresponding to the spatial distribution of trajectory frequency, Central Siberia and Lake Baikal are identified as the important common key areas for CAOs affecting six subregions. For the CAO in North China, cold air parcels were highly intensified within a short period from around −5 to −3 d over the southwestern side of Lake Baikal. By contrast, for the CAO in Northeast China, cold air parcels accumulated over a broad area from west of Lake Baikal to the Northeast Plain during a relatively long period from −8 to −2 d. The Turpan Basin and the Hetao Plain were the particular key areas for the cooling of cold air parcels reaching Central China, whilst the Junggar Basin was for the cold air parcels arriving in Northwest China. Cold air parcels that hit East China underwent multiple cooling accumulation processes from −10 to −4 d over Central Siberia, western and southern Lake Baikal, as well as in the eastern part of the Inner Mongolia Plateau and the North China Plain. Further intensification of cold air parcels over the North China Plain allowed the penetration of cold air parcels further south into Central and South China in 1−2 d, with a relatively mild cooling. Therefore, the North China Plain is also the common key area for the intensification of cold air parcels reaching Central, East and South China.

4. Discussion and conclusions

From 26 November to 1 December 2022, extremely cold air rapidly swept across China from the northwest to the south. Six subregions were divided to identify and track this CAO in the Lagrangian backward tracking framework with the HYSPLIT model. The DSE concept was adopted to investigate the evolution (i.e. intensification or weakening) of cold air parcels. To reveal the dominant processes leading to CAOs for different subregions, the DSE change along the trajectory was decomposed into four diabatic heating terms (i.e. shortwave radiation, longwave radiation, latent heat and turbulent processes), with the methodology in the spirit of You et al. (2021) and Hartig et al. (2023). The main findings are summarised as follows.

In this CAO case, most cold air parcels originate east of Novaya Zemlya and then pass through Central Siberia before reaching China. Hence, these air parcels mainly manifest on the northwest-to-southeast path, with the exception of Northwest China, which is roughly a north-to-south path due to its shorter distance from Central Siberia.

For different subregions, the time spans of cold air intensification, which are indicated by the period from −10 d to the moment of the minimum DSE and the associated DSE change, representing the degree of intensification due to diabatic processes, are different. The cold air parcels reaching northern China (i.e. Northwest, North and Northeast China) undergo long intensification periods of almost 9 d before their outbreak, with a cooling of >12.0 K. By contrast, the cooling periods of those arriving in the southern parts (i.e. Central, East and South China) are noticeably short (6−8 d). Particularly, the DSE of air parcels in South and East China was reduced to a lesser extent <6.0 K.

The four temperature tendencies from the distinct diabatic processes (longwave cooling, shortwave warming, latent heat release and turbulent processes) were interpolated onto each trajectory simulated by the HYSPLIT model. The interpolation results indicate that longwave radiative cooling is the dominant contributor to diabatic temperature evolution,

Please cite this article as: CHE, J.-N et al., Understanding the physical processes in the evolution of a cold air outbreak over China in late November 2022 from a Lagrangian perspective, Advances in Climate Change Research, https://doi.org/10.1016/j.accre.2023.08.009

causing an average cumulative cooling of approximately 20 K along the trajectories arriving at each region. Latent heat release is nearly negligible. Whereas shortwave radiative heating of the air parcel and the turbulence term serve to counteract the strengthening of cold air parcels.

To distinguish the key areas where cold air parcels are enhanced (cooled), the DSE change at each grid for all trajectories passing through this grid was accumulated as the total contribution to the intensification of cold air parcels. Central Siberia and Lake Baikal are identified as the common key areas of the cold air intensification for all six subregions. The North China Plain is the common key area for the intensification of cold air parcels reaching Central, East and South China.

Overall, the results in the framework of Lagrangian backward tracking are obtained on the basis of the combination of the observational (reanalysis) datasets with the decomposition of temperature tendencies along the trajectory. We have identified the main pathways of this CAO and, in particular, the dominant diabatic processes contributing to the accumulation of the cold air parcel, and further revealed the periods and regions, when and where the cold air parcel was intensified. These findings provide new insights into the physical mechanisms that drive the behaviour of cold air parcels and hence shed light on the prediction of CAO. In addition, the results are currently confined to a single CAO case, and some uncertainty and limitations inevitably exist. The main uncertainty in using Eq. (4) should be considered because the contribution of the residual term ($\Delta\mathrm{DSE} - \int \dot{T}_{\mathrm{Physics}} \mathrm{d}t$), which may be due to the multiple interpolation processes and the uncertainty in the ERA5 temperature tendency data itself, is occasionally not negligible (Fig. 5g). On a global scale, the specific adiabatic processes that dominate the temperature change of cold air parcels may vary from region to region and from case to case for individual CAOs if they are investigated by using the methodology adopted in this study.

A reliable future projection of CAOs would help mitigate the associated damages. However, under the global warming of the past decades, the reported changes in the frequency, intensity and duration of CAOs in numerous studies (Dai et al., 2022; Ding et al., 2021; Overland et al., 2016; Yao et al., 2022, 2023; Zhou et al., 2022) are inconsistent, with a slight increase in some investigations (Liu et al., 2012; Cohen et al., 2014) while an apparent decrease in others (Vavrus et al., 2006; Smith and Sheridan, 2020). Using this approach to investigate the underlying mechanism behind the changes in CAO would help reconcile the seemingly inconsistent past trends between these studies, and thus provide an important basis for their future projections.

Declaration of competing interest

The authors declare no conflict of interest.

Acknowledgments

This work was supported by the National Nature Science Foundation of China (41875119, 42005118 and 42375037), Science and Technology Development Plan in Jilin Province of China (20230203135SF) and Open Research of State Key Laboratory of Severe Weather (2022LASW-B05). The authors thank Dr. Ning Hu and Dr. Xiaofang Wang for their help with the methodology and dataset.

References

Cai, B., Zeng, G., Zhang, G., et al., 2019. Autumn cold surge paths over North China and the associated atmospheric circulation. Atmosphere 10, 134. https://doi.org/10.3390/atmos10030134.

CMA (China Meteorological Administration), 2023. China Climate Bulletin 2022. http://www.cma.gov.cn/root7/auto13139.

CMA, 2017. Grades of Cold Wave (GB/T 21987-2017). Standards Press of China, Beijing (Chinese).

Cohen, J., Screen, J., Furtado, J., et al., 2014. Recent Arctic amplification and extreme mid-latitude weather. Nat. Geosci. 7, 627–637. https://doi.org/10.1038/ngeo2234.

Dai, G., Mu, M., 2020. Arctic influence on the eastern Asian cold surge forecast: a case study of January 2016. J. Geophys. Res. Atmospheres 125 (23), e2020JD033298. https://doi.org/10.1029/2020JD033298.

Dai, G., Coauthors, 2022. The nature and predictability of the East Asian extreme cold events of 2020/21. Adv. Atmos. Sci. 39, 566–575. https://doi.org/10.1007/s00376-021-1057-3.

Ding, Y.H., Ma, X.Q., 2007. Analysis of isentropic potential vorticity for a strong cold wave in 2004/2005 winter. Acta Meteorol. Sin. 65, 695–707. https://doi.org/10.11676/qxxb2007.065 (Chinese.

Ding, Y.H., Wang, Z.Y., Song, Y.F., et al., 2008. Causes of the unprecedented freezing disaster in January 2008 and its possible association with the global warming. Acta Meteorol. Sin. 22, 538–558. https://doi.org/10.11676/qxxb2008.074.

Ding, T., Gao, H., Li, X., 2021. Increasing occurrence of extreme cold surges in North China during the recent global warming slowdown and the possible linkage to the extreme pressure rises over Siberia. Atmos. Res. 248, 105198. https://doi.org/10.1016/j.atmosres.2020.105198.

Draxler, R.R., Hess, G.D., 1997. Description of the HYSPLIT_4 modeling system. NOAA Tech. Memo. ERL ARL- 224, 24. https://doi.org/10.1016/S0140-6736(02)98733-7.

Draxler, R.R., Hess, G., 1998. An overview of the HYSPLIT_4modelling system for trajectories. Aust. Meteor. Mag. 47, 295–308.

Gong, Z.Q., Feng, G.L., Ren, F.M., et al., 2014. A regional extreme low temperature event and its main atmospheric contributing factors. Theor. Appl. Climatol. 117, 195–206. https://doi.org/10.1007/s00704-013-0997-7.

Hartig, K., Tziperman, E., Loughner, C.P., 2023. Processes contributing to North American cold air outbreaks based on air parcel trajectory analysis. J. Clim. 36 (3), 931–943. https://doi.org/10.1175/JCLI-D-22-0204.1.

Hermann, M., Papritz, L., Wernli, H., 2020. A Lagrangian analysis of the dynamical and thermodynamic drivers of large-scale Greenland melt events during 1979–2017. Weather Clim. Dynam. 1 (2), 497–518. https://doi.org/10.5194/wcd-1-497-2020.

Hersbach, H., Bell, B., Berrisford, P., et al., 2020. The Era5 global reanalysis. Q. J. R. Meteorol. Soc. 146, 1999–2049.

Hoskins, B.J., McIntyre, M.E., Robertson, A.W., 1985. On the use and significance of isentropic potential vorticity maps. Q. J. R. Meteorol. Soc. 111, 877–946. https://doi.org/10.1002/qj.49711147002.

Huang, J.L., Hitchcock, P., Maycock, A.C., et al., 2021. Northern Hemisphere cold air outbreaks are more likely to be severe during weak polar vortex conditions. Commun. Earth Environ. 2, 147. https://doi.org/10.1038/s43247-021-00215-6.

Huang, W.Y., Dong, W., Shen, X.Y., et al., 2020. Isentropic vortex and thermodynamic analysis of a cold wave cooling process. J. Atmos. Sci. 40 (6), 769–781. https://doi.org/10.3969/2019jms.0028.

Iwasaki, T., Shoji, T., Kanno, Y., et al., 2014. Isentropic analysis of polar cold air mass streams in the Northern Hemispheric winter. J. Atmos. Sci. 71, 2230–2243. https://doi.org/10.1175/JAS-D-13-058.1.

Please cite this article as: CHE, J.-N et al., Understanding the physical processes in the evolution of a cold air outbreak over China in late November 2022 from a Lagrangian perspective, Advances in Climate Change Research, https://doi.org/10.1016/j.accre.2023.08.009

Li, J., Xie, T., Tang, X., et al., 2022. Influence of the NAO on wintertime surface air temperature over East Asia: multidecadal variability and decadal prediction. Adv. Atmos. Sci. https://doi.org/10.1007/s00376-021-1075-1.

Li, X., Zhang, Y.J., Gao, H., 2022. The extreme cold wave in early November 2021 in China and the influences from the meridional pressure gradient over East Asia. Adv. Clim. Change Res. 13 (6), 797e802. https://doi.org/10.1016/j.accre.2022.11.011.

Liu, C.Y., Lu, B., Jin, L., et al., 2022. Impact of the cold surge event in January 2021 on the power system of China. Adv. Clim. Change Res. 13 (6), 803e810. https://doi.org/10.1016/j.accre.2022.11.004.

Liu, J., Curry, J., Wang, H., et al., 2012. Impact of declining Arcticsea ice on winter snowfall. Proc. Natl. Acad. Sci. U.S.A. 109, 4074–4079. https://doi.org/10.1073/pnas.1114910109.

Liu, Q., Liu, Q., Chen, G., 2020. Isentropic analysis of regional cold events over northern China. Adv. Atmos. Sci. 37, 718–734. https://doi.org/10.1007/s00376-020-9226-3.

Luo, D.H., Zhang, W.Q., Zhong, L.H., et al., 2019. A nonlinear theory of atmospheric blocking: a potential vorticity gradient view. J. Atmos. Sci. 76, 2399–2427. https://doi.org/10.1175/JAS-D-18-0324.1.

Luo, J., Chen, H., Zhou, B., 2020. Comparison of snowfall variations over China identified from different snowfall/rainfall discrimination methods. J. Meteorol. Res. 34, 1114. https://doi.org/10.1007/s13351-020-0004-z, 28.

Ma, S.M., Zhu, C.W., 2019. Extreme cold wave over East Asia in January 2016: a possible response to the larger internal atmospheric variability induced by Arctic warming. J. Clim. 32 (4), 1203e1216. https://doi.org/10.1175/JCLI-D-18-0234.1.

NRC (National Report Committee), 2007. China's National Assessment Report on Climate Change. Science Press, Beijing (Chinese).

Overland, J., Dethloff, K., Francis, J., et al., 2016. Nonlinear response of mid-latitude weather to the changing Arctic. Nat. Clim. Change 6 (11), 992–999. https://doi.org/10.1038/nclimate3121.

Papritz, L., Spengler, T., 2017. A Lagrangian climatology of wintertime cold air outbreaks in the Irminger and Nordic Seas and their role in shaping air–sea heat fluxes. J. Clim. 30 (8), 2717–2737. https://doi.org/10.1175/JCLI-D-16-0605.1.

Papritz, L., Pfahl, S., Sodemann, H., et al., 2015. A climatology of cold air outbreaks and their impact on air–sea heat fluxes in the High-Latitude South Pacific. J. Clim. 28 (1), 342–364. https://doi.org/10.1175/JCLI-D-14-00482.1.

Screen, J., Simmonds, I., 2014. Amplified mid-latitude planetary waves favour particular regional weather extremes. Nat. Clim. Change 4, 704–709. https://doi.org/10.1038/nclimate2271.

Shoji, T., Kanno, Y., Iwasaki, T., et al., 2014. An isentropic analysis of the temporal evolution of East Asian cold air outbreaks. J. Clim. 27, 9337–9348. https://doi.org/10.1175/JCLI-D-14-00307.1.

Smith, E., Sheridan, S., 2020. Where do cold air outbreaks occur, and how have they changed over time? Geophys. Res. Lett. 47, e2020GL086983. https://doi.org/10.1029/2020GL086983.

Stein, A., Draxler, R., Rolph, G., et al., 2015. NOAA's HYSPLIT atmospheric transport and dispersion modeling system. Bull. Am. Meteorol. Soc. 96, 2059–2077. https://doi.org/10.1175/BAMS-D-14-00110.1.

Sun, Y., Hu, T., Zhang, X.B., et al., 2018. Anthropogenic influence on the eastern China 2016 super cold surge Bam. Meteorol. Soc. 99 (1), S123–S127. https://doi.org/10.1175/BAMS-D-17-0092.1.

Sun, Z., Wang, Z., Zeng, G., 2017. The characteristics of cold air outbreaks in Northwest China based on airflow trajectory model. J. Zhengzhou Univ. 49, 1671–6841. https://doi.org/10.13705/j.issn.1671-6841.2017064 (Chinese.

Tao, Z., Zheng, Y., 2012. Analysis methods on potential temperature, isentropic potential vorticity. front and tropopause. Meteor. Mon. 38 (1), 17–27. https://doi.org/10.7519/j.issn.1000-0526.2012.01.002.

Vavrus, S., Walsh, J., Chapman, W., et al., 2006. The behavior of extreme cold air outbreaks under greenhouse warming. Int. J. Climatol. 26 (9), 1133–1147. https://doi.org/10.1002/joc.1301.

Wallace, J., Held, I., Thompson, D.W.J., et al., 2014. Global warming and winter weather. Science 343, 729–730. https://doi.org/10.1126/science.343.6172.729.

Walsh, J., Phillips, A., Portis, D., et al., 2001. Extreme cold outbreaks in the United States and Europe, 1948–99. J. Clim. 14 (12), 2642–2658. https://doi.org/10.1175/1520-0442(2001)014<2642:ECOITU>2.0.CO;2.

Wang, Z., Sun, Z., Zeng, G., 2017. Characteristics of strong cold air outbreaks in Northeast China during 1970 to 2013. J. Xinyang Norm. Univ. 30, 407–411. https://doi.org/10.3969/j.issn.1003-0972.2017.03.013 (Chinese).

Yamaguchi, J., Kanno, Y., Chen, G., Iwasaki, T., 2019. Cold air mass analysis of the record-breaking cold surge event over East Asia in January 2016. J. Meteorol. Soc. Jpn. 97, 275–293. https://doi.org/10.2151/jmsj.2019-015.

Yao, Y., Zhuo, W., Gong, Z., et al., 2023. Extreme cold events in North America and Eurasia in November–December 2022: a potential vorticity gradient perspective. Adv. Atmos. Sci. 40, 953–962. https://doi.org/10.1007/s00376-023-2384-3.

Yao, Y., Zhang, W., Luo, D., et al., 2022. Seasonal cumulative effect of ural blocking episodes on the frequent cold events in China during the early winter of 2020/21. Adv. Atmos. Sci. 39, 609–624. https://doi.org/10.1007/s00376-021-1100-4.

You, C., Tjernström, M., Devasthale, A., 2020. Warm-air advection over melting sea-ice: a Lagrangian case study. Bound-Lay Meteorol. 179, 99–116. https://doi.org/10.1007/s10546-020-00590-1.

You, C., Tjernström, M., Devasthale, A., 2021. Eulerian and Lagrangian views of warm and moist air intrusions into summer Arctic. Atmos. Res. 256, 105586. https://doi.org/10.1016/j.atmosres.2021.105586.

You, C., Tjernström, M., Devasthale, A., 2022. Warm and moist air intrusions into the winter Arctic: a Lagrangian view on the near-surface energy budgets. Atmos. Chem. Phys. 22, 8037–8057. https://doi.org/10.5194/acp-22-8037-2022.

Zhang, Y., Wang, G., 2022. Assessment of the hazard of extreme low-temperature events over China in 2021. Adv. Clim. Change Res. 13 (6), 811e818. https://doi.org/10.1016/j.accre.2022.11.005.

Zhou, T., Zhang, W., Zhang, L., et al., 2022. 2021: a year of unprecedented climate extremes in eastern Asia, North America, and Europe. Adv. Atmos. Sci. 39, 1598–1607. https://doi.org/10.1007/s00376-022-2063-9.

Please cite this article as: CHE, J.-N et al., Understanding the physical processes in the evolution of a cold air outbreak over China in late November 2022 from a Lagrangian perspective, Advances in Climate Change Research, https://doi.org/10.1016/j.accre.2023.08.009